Acta Crystallographica Section D
Biological Crystallography
ISSN 0907-4449

Phase changes in $T_3R_3^f$ human insulin: temperature or pressure induced?

G. David Smith,[a,b]* Walter A. Pangborn[a] and Robert H. Blessing[a]

[a]Hauptman–Woodward Medical Research Institute, 73 High Street, Buffalo, NY 14203, USA, and [b]Roswell Park Cancer Institute, Elm and Carlton Streets, Buffalo, NY 14263, USA

Correspondence e-mail: smith@hwi.buffalo.edu

Received 6 December 2000
Accepted 9 May 2001

PDB References: 1.2 Å $T_3R_3^f$ insulin, 1g7a; 1.3 Å $T_3R_3^f$ insulin, 1g7b.

The structure of $T_3R_3^f$ hexameric human insulin has been determined at 100 K from two different crystals at 1.2 and 1.3 Å resolution and refined to residuals of 0.169 and 0.176, respectively. Owing to a phase change, the *c* axis is double its room-temperature value and the asymmetric unit contains two independent TR^f insulin dimers. Compared with the orientation in the room-temperature structure, one dimer undergoes a rotation about the *c* axis of −5°, while the second is rotated +4°. A superposition of the backbone atoms of the two independent dimers shows that the C^α atoms of five residues within the R^f-state monomers are displaced by more than 1.0 Å; smaller displacements are observed for the T-state monomers. Four zinc ions lie on the crystallographic threefold axis and each forms bonds to three symmetry-related HisB10 $N^{\varepsilon 2}$ atoms from the T- and R^f-state trimers. While three of the zinc ions are tetrahedrally coordinated with a chloride ion completing the coordination sphere, mixed tetrahedral/octahedral coordination is observed for one of the T-state zinc ions. The three symmetry-related 'phenolic binding sites' in one hexamer contain water molecules and a glycerol molecule, but the same sites in the second hexamer are occupied by a zinc ion coordinated to an alternate conformation of HisB10, a symmetry-related HisB5 and two chloride ions. Two additional and partially occupied zinc ion sites are observed at the interface between the two independent dimers. One zinc ion is coordinated by a T-state HisB5 of one dimer, an R-state HisB5 of the second dimer and two water molecules; the second zinc ion is coordinated by an alternate side-chain conformation of the T-state HisB5 and three water molecules. The carboxyl group of one GluB13 side chain, which exists in two discrete conformations, appears to be protonated, because short contacts exist to a second carboxyl group or to a carbonyl O atom.

1. Introduction

The allosteric nature of hexameric insulin was first observed by Schlichtkrull (1958) when he found that a second rhombohedral crystal form was produced when the chloride ion content exceeded 6% in the crystallization media. This form of insulin was originally named 4-zinc insulin (Bentley *et al.*, 1976) as it contained four zinc ions per hexamer compared with two zincs observed in the original hexameric insulin structure (Adams *et al.*, 1969). Accompanying the increase in zinc content in the 4-zinc structure was a conformational change from extended to α-helical in residues 4–8 in the B chains in one insulin trimer. As additional allosteric forms of hexameric insulin have been found with varying zinc content,

the T and R nomenclature (Kaarsholm *et al.*, 1989) has been adopted, where T represents an extended conformation of the first eight residues in the B chain and R an α-helical conformation, producing a continuous α-helix from residue PheB1 to CysB19. R^f represents a 'frayed' α-helix in which residues B1 through B3 are extended and the segment from GlnB4 to CysB19 is α-helical (Ciszak *et al.*, 1995). In this nomenclature, the original 2-zinc insulin hexamer is referred to as T_6, while the form obtained in the presence of high chloride ion concentration (4-zinc insulin) is $T_3R_3^f$. While ions such as chloride (Bentley *et al.*, 1976; Ciszak & Smith, 1994) or thiocyanate (Whittingham *et al.*, 1995) are capable of inducing the T→R transition in three monomers in the hexamer, only phenolic derivatives such as phenol (Derewenda *et al.*, 1989; Smith & Dodson, 1992), *m*-cresol or resorcinol (Smith *et al.*, 2000) are capable of producing an R_6 hexamer. Some other phenolic derivatives such as 4′-hydroxyacetanilide, *p*-hydroxybenzamide and methylparaben (Smith & Ciszak, 1994; Smith *et al.*, 1996; Whittingham *et al.*, 1995) are incapable of driving the T→R transition to completion and only $T_3R_3^f$ hexamers are produced. As the N terminus of the B chain undergoes the conformational change, an elliptical cavity is produced between symmetry-related monomers (Smith, 1998). In the presence of phenolic derivatives, this cavity is occupied by the phenolic derivative and the phenolic hydroxy group forms hydrogen bonds to the carbonyl O atom of CysA6 and the N atom of CysA11. In the absence of phenolic derivatives, the cavity is occupied by either water molecules (Ciszak & Smith, 1994; Whittingham *et al.*, 1995) or by zinc ions (Bentley *et al.*, 1976; Smith *et al.*, 1984).

The structure of $T_3R_3^f$ human insulin has also been determined at room temperature by powder diffraction methods (Von Dreele *et al.*, 2000). Owing to pressure resulting from the mechanical grinding of the polycrystalline sample, the *c* axis was found to be double that reported from room-temperature single-crystal studies (Ciszak & Smith, 1994; Whittingham *et al.*, 1995). However, the structure of the ground powder sample reverted to its original form after several days. Reported here are the 1.2 and 1.3 Å resolution structure of $T_3R_3^f$ human insulin at 100 K derived from crystals grown in microgravity. As a result of cryocooling, the *c* axis is doubled as was observed in the room-temperature powder diffraction studies, producing two independent TR^f dimers in the asymmetric unit.

2. Experimental

2.1. Crystallization

Biosynthetic human insulin complexed with zinc was provided by Lilly Research Laboratories. Buffer, salts and other reagents were purchased and used without further purification. Crystals were grown in microgravity aboard shuttle flight STS-95 using the UAB PCF (University of Alabama at Birmingham Protein Crystallization Facility) apparatus and a solution containing 5 mg ml^{-1} insulin, 0.01 *M* HCl, 0.007 *M* zinc acetate, 0.05 *M* sodium citrate, 17% acetone, 1.0 *M* NaCl at a pH of 6.3. The crystals grown in microgravity were free of inclusions, very well formed and of a nearly uniform size of 0.4 mm along an edge, but the ground-control crystals were deemed unusable for single-crystal studies.

Table 1
Data-measurement statistics for crystals 1 and 4 of $T_3R_3^f$ human insulin.

	Crystal 1	Crystal 4
Space group	*R*3	*R*3
Unit-cell parameters		
a (Å)	80.05	80.13
b (Å)	80.05	80.13
c (Å)	71.46	71.58
α (°)	90.0	90.0
β (°)	90.0	90.0
γ (°)	120.0	120.0
Temperature (K)	100	100
B_{iso} (Å^2)	19.4	17.6
No. of frames	353	340
Resolution (Å)	1.30	1.20
Total data	912730	925256
Unique data	41901	53700
Average redundancy	12.5	8.6
Completeness (%)	100.0	100.0
Total missing data	6	7
Overall R_{merge}	0.060	0.049
$\langle F^2\rangle/\sigma\langle F^2\rangle$	48.8	42.8
Resolution (final shell)	1.33–1.30	1.23–1.20
Completeness (%)	100.0	100.0
$\langle F^2\rangle/\langle\sigma(F^2)\rangle > 3$ (%)	79.4	75.9
$\langle F^2\rangle/\langle\sigma(F^2)\rangle$	8.6	7.1
R_{merge}	0.393	0.299

2.2. Data measurement

Following cryoprotection with mother liquor and a mixture of glycerol and PEG 400, the crystals were looped and flash-frozen at liquid-nitrogen temperatures. Data were measured at 100 K with λ = 0.8000 Å from two different crystals, one from a 50 ml PCF vial and one from a 10 ml PCF vial, using an ADSC Quantum 4 detector at beamline X8-C of the National Synchrotron Light Source, Brookhaven National Laboratory. Integration, scaling and merging of the data were performed with *DENZO* and *SCALEPACK* (Otwinowski & Minor, 1997). The independent data from each crystal were then processed further with *SORTAV*, *BAYES* and *LEVY* (Blessing, 1997) to reformat the data, to apply Bayesian statistics to the weak data and to estimate the scale factor and overall isotropic temperature factor, respectively. Unit-cell, space-group and data statistics are given in Table 1.

In order to compare the data from cryofrozen crystals with those at room temperature, a single crystal grown in microgravity with a largest dimension of 0.4 mm was mounted in a quartz capillary along with a drop of mother liquor and a complete data set was measured at room temperature on a Rigaku R-AXIS IV and RU-200 rotating-anode generator equipped with Osmic confocal mirrors. Unit-cell parameters were found to be equivalent to previously published structures (PDB entry 1trz), $a = 80.89$, $c = 37.59$ Å; 54% of the data in the highest resolution shell, 1.86–1.80 Å resolution, had F^2 greater than $3\sigma(F^2)$.

We hypothesized that if the phase change is pressure induced, resulting from the contraction of the drop of frozen cryoprotectant which surrounds the crystal in the loop, then replacing the cryoprotectant drop by a thin layer of paraffin oil might reduce any effects owing to pressure. For this reason, four crystals were immersed in paraffin oil, excess oil was removed and preliminary diffraction data were measured at 100 K on an R-AXIS IV^{++} equipped with Osmic confocal mirrors and an Xtreme cryosystem. The *c* axis of all four crystals was found to be doubled, indicating that the phase transition had occurred in the absence of the cryoprotectant drop.

2.3. Structure solution and refinement

2.3.1. Crystal 4. The structure was solved by molecular replacement using *CNS* (DeLano & Brünger, 1995) and the 1.2 Å resolution data. The model was constructed from PDB entry 1trz (Ciszak & Smith, 1994) from which disordered side chains, all water molecules, zinc and chloride ions were removed; the second independent dimer was generated by adding one half of the *c*-axis dimension to the *z* parameter of each atom of dimer 1. Each atom was assigned the temperature factor obtained from Wilson analysis in the program *LEVY*. 10% of the data were reserved for cross validation and were never used during structure solution or refinement (Brünger, 1992). A translation-function search was performed using the coordinates from the best solution from the rotation function using data between 15.0 and 4.0 Å resolution. Rigid-body refinement using *CNS* with an overall anisotropic temperature factor and a bulk-solvent correction (Brunger *et al.*, 1998; Pannu & Read, 1996; Adams *et al.*, 1997), treating each independent dimer as a single rigid body, produced values of 0.397 and 0.409 for *R* and $R_{\rm free}$, respectively, for data between 80.0 and 2.0 Å resolution. The σ_A-weighted $(2F_o - F_c)$ and $(F_o - F_c)$ maps (Read, 1986; Brünger *et al.*, 1997) were calculated and, using *CHAIN* (Sack, 1988), clearly indicated the positions of all four axial zinc and chloride ions. These atoms were included in the model and one cycle of maximum-likelihood torsion-angle dynamics, conjugate-gradient refinement and grouped temperature-factor refinement (Rice & Brünger, 1994; Brunger *et al.*, 1998; Adams *et al.*, 1997; Pannu & Read, 1996) reduced the *R* factor to 0.262 and $R_{\rm free}$ to 0.276 for data between 80.0 and 1.2 Å resolution. Bonds involving zinc ions were not restrained. Examination of the σ_A-weighted maps clearly indicated the presence of another zinc ion in the off-axial binding site (phenolic binding site) of dimer 1, where it is coordinated by a second orientation of HisB10.2,[1] HisB5.2 of an adjacent symmetry-related monomer and two chloride ions. The electron density in the off-axial binding site in dimer 2 did not indicate an additional zinc ion, but rather several disordered water molecules and one glycerol molecule. Two additional zinc ions were located between pairs of independent dimers whose *z* parameters differ by one half of the *c* dimension. The refinement was continued and σ_A-weighted $(2F_o - F_c)$ and $(F_o - F_c)$ maps were examined at the end of each round of refinement. Adjustments were made to main-chain and side-chain atoms, additional groups were added as necessary and water molecules were added in accord with good electron density and the formation of hydrogen bonds to known atoms. Two acetone molecules were also identified from the electron densities; they were assigned as acetone rather than acetate owing to the lack of hydrogen-bonding opportunities to the two putative methyl groups. During the course of the refinement, protein H atoms were added and refined. The geometry was continually monitored with *PROCHECK* (Laskowski *et al.*, 1993) throughout the course of the refinement.

Table 2
Data-refinement statistics for crystals 1 and 4 of $T_3R_3^f$ human insulin.

	Crystal 1	Crystal 4
No. of reflections	41901	53646
Resolution range (Å)	31.8–1.3	31.2–1.2
R value	0.176	0.169
$R_{\rm free}$ value	0.204	0.193
Highest resolution shell		
Resolution range (Å)	1.38–1.30	1.28–1.20
No. of reflections	6219	8098
Completeness (%)	100.0	100.0
R value	0.209	0.240
$R_{\rm free}$ value	0.236	0.259
Cross-validated estimated error (Å)	0.09	0.12
R.m.s. deviations from ideal		
Bond lengths (Å)	0.010	0.009
Bond angles (°)	1.92	1.88
Dihedral angles (°)	20.4	20.6
Improper angles (°)	0.89	0.92
Isotropic thermal model restraints		
Main-chain bonds (Å^2)	1.87	1.98
Main-chain angles (Å^2)	2.66	2.74
Side-chain bonds (Å^2)	2.16	2.29
Side-chain angles (Å^2)	2.73	2.80

At the conclusion of the refinement, the final model contained 1575 non-H protein atoms, two acetone molecules, one glycerol molecule, 213 water molecules with occupancies of unity, 122 water molecules with partial occupancies, seven zinc ions and seven chloride ions. A total of 16 side chains were found to adopt two distinct conformations: HisB5.1, ThrB27.1, GlnA5.2, ThrA8.2, GluA17.2, PheB1.2, HisB10.2, GluB13.2, GluB21.2, GlnA5.3, SerA9.3, ValB12.3, IleA10.4, GluB13.4, PheB25.4 and ThrB27.4. The N-terminal residue, PheB1.4, could not be located, the electron density for residues B2.4 and B3.4 was poor and the side chains of ValB2.4 and GlnB4.2 could not be located. While complete residues could be modeled for LysB29.3 and ThrB30.3, no density was present for ThrB30.2 and ThrB30.4, nor for the side chains of LysB29.2 and LysB29.4. Although side-chain density was absent for LysB29.1 and ThrB30.1, the main-chain atoms were modeled in two distinct conformations. Refinement statistics are given in Table 2.

2.3.2. Crystal 1. Even though this crystal did not diffract quite as well as crystal 4, the structure was independently refined in order to verify various features of the previously

[1] The decimal portion of the residue number, 0.1 through 0.4, refers to the monomer number in the two independent dimers.

Table 3
Dimer-forming, hexamer-forming and hexamer–hexamer hydrogen-bonded contacts in the present study and in 1trz.

Atom 1	Atom 2	Dist. (Å)	Dist. 1trz (Å)	Symmetry	
Dimer-forming hydrogen bonds					
GluB13.1 $O^{\varepsilon1}$	SerB9.2 O^{γ}	3.10	2.90		
GluB13.1 $O^{\varepsilon1}$	GluB13.2 $O^{\varepsilon2}$ *B*†	3.17	3.07		
TyrB16.1 O^{η}	HisB5.2 O	2.62	2.82		
PheB24.1 N	TyrB26.2 O	3.10	2.89		
PheB24.1 O	TyrB26.2 N	2.75	2.80		
TyrB26.1 N	PheB24.2 O	2.89	2.93		
TyrB26.1 O	PheB24.2N	2.88	2.92		
SerB9.3 O	GluB13.4 $O^{\varepsilon1}$	3.04	6.40		
SerB9.3 O	GluB13.4 $O^{\varepsilon2}$	2.73	4.78		
GluB13.3 $O^{\varepsilon2}$	SerB9.4 O^{γ}	2.84	2.52, 2.85‡		
TyrB16.3 O^{η}	HisB5.4 O	2.71	2.82		
PheB24.3 N	TyrB26.4 O	2.95	2.89		
PheB24.3 O	TyrB26.4 N	2.88	2.80		
TyrB26.3 N	PheB24.4 O	2.86	2.93		
TyrB26.3 O	PheB24.4N	2.89	2.92		
Hexamer-forming hydrogen bonds					
ValB2.1 N	LeuB17.2 O	2.87	2.78	$y-x, -x, z$	0, 0, 0
GlnB4.1 $O^{\varepsilon1}$	TyrB16.2 O^{η}	2.60	2.64	$y-x, -x, z$	0, 0, 0
PheB1.3 N	ValB18.4 O	2.98	3.26	$y-x, -x, z$	0, 0, 0
ValB2.3 N	LeuB17.4 O	2.85	2.78	$y-x, -x, z$	0, 0, 0
GlnB4.3 $O^{\varepsilon1}$	TyrB16.4 O^{η}	2.56	2.64§	$y-x, -x, z$	0, 0, 0
GluB13.3 $O^{\varepsilon2}$	GluB13.4 $O^{\varepsilon1}$ *B*†	2.54	5.18	$y-x, -x, z$	0, 0, 0
Hexamer–hexamer hydrogen bonds					
ThrA8.1 $O^{\gamma1}$	GluA4.4 $O^{\varepsilon2}$	2.77	4.70	x, y, z	0, 0, −1
GlyA1.1 N	GluA17.4 $O^{\varepsilon2}$	2.83	3.94	$-y, x-y, z$	−2/3, 2/3, −1/3
Thr B27.1 $O^{\gamma1}$	AsnA18.4 $O^{\delta1}$	2.74	2.79	$-y, x-y, z$	−2/3, 2/3, −1/3
ThrB27.1 $O^{\gamma1}$ *B*†	AsnA18.4 $O^{\delta1}$	2.77	2.70	$-y, x-y, z$	−2/3, 2/3, −1/3
ThrB30.1 O	GluA17.4 $O^{\varepsilon2}$	2.99	5.37	$-y, x-y, z$	−2/3, 2/3, −1/3
ThrB30.1 O	ArgB22.4 $N^{\eta1}$	3.11	3.78	$-y, x-y, z$	−2/3, 2/3, −1/3
GlnA5.1 $O^{\varepsilon1}$	TyrA14.3 O^{η}	2.94	3.04	$y-x, -x, z$	−2/3, 2/3, −1/3
ThrA8.2 O	HisB5.3 $N^{\varepsilon2}$	2.48	2.80	$-y, x-y, z$	0, 0, 0
ThrA8.2 O *B*†	HisB5.3 $N^{\varepsilon2}$	2.57	¶	$-y, x-y, z$	0, 0, 0
GluA17.2 $O^{\varepsilon2}$	GlyA1.3 N	2.74	3.68	$y-x, -x, z$	−1/3, −2/3, −2/3
AsnA18.2 O	LysB29.3 N^{ζ}	2.85	††	$y-x, -x, z$	−1/3, −2/3, −2/3
CysA20.2 O	LysB29.3 N^{ζ}	2.83	††	$y-x, -x, z$	−1/3, −2/3, −2/3

† *B* signifies a second orientation of a side chain. ‡ There are two side-chain conformations for SerB9.2 in 1trz. § This is GlnB4.1 $N^{\varepsilon2}$ in 1trz. ¶ There is no second side-chain conformation of ThrA8.2 in 1trz. †† Lysine side chains were not located in 1trz.

refined structure. 10% of the data were reserved for cross validation and were never used during the refinement. Starting coordinates consisted of the refined protein atoms from crystal 4 with disordered side chains truncated to alanine and all water molecules, zinc and chloride ions and other groups excluded. A single round of refinement using maximum-likelihood torsion-angle dynamics and grouped temperature-factor refinement reduced the *R* factor to 0.292 and $R_{\rm free}$ to 0.310. The refinement was continued as described above. At the end of the refinement, the final model contained 1575 non-H protein atoms, one acetone molecule, one glycerol molecule, 158 water molecules with occupancies of unity, 83 water molecules with partial occupancies, seven zinc ions and seven chloride ions. A total of ten side chains were found to adopt two distinct conformations: HisB5.1, ThrB27.1, GluA17.2, HisB10.2, GluB13.2, SerA9.3, ValB12.3, IleA10.4, GluB13.4 and ThrB27.4. The electron density for the N-terminal B-chain residue of monomer 4 was weak and nearly identical to that observed for crystal 4, as were all four of the C-terminal B-chain residues. Refinement statistics are given in Table 2.

3. Discussion

A comparison of the refined structures from crystals 1 and 4 reveals few significant differences in structure or conformation. Superposition by a least-squares procedure (Smith, 1993) of the backbone atoms in both dimers yielded a mean displacement of 0.079 Å, with the largest C^{α} displacement being 0.397 Å at ThrA8.2. Only eight C^{α} atoms had displacements larger than 0.20 Å. Of the 234 water molecules which are in common between the two structures, a mean displacement of 0.19 Å was calculated. Given the similarity of the two structures and the difference in resolution, the following discussion will focus on the structure obtained from crystal 4. The structure of the pair of independent dimers is illustrated in Fig. 1.

A superposition of all backbone atoms onto the structure obtained from the powder diffraction studies, PDB entry 1fu2 (Von Dreele *et al.*, 2000), produced a mean C^{α} displacement of 1.36 Å (r.m.s. displacement = 1.53 Å), which is insignificant given that the resolution of the powder diffraction study was 3.24 Å. The largest C^{α} displacement was 5.91 Å at B30.1Thr, while the second and third largest were 4.81 Å at A1.4Gly and 3.59 Å at A5.4Glu, respectively. Numerous large differences in conformation are observed for the side chains, but this is probably a consequence of the low resolution of the powder diffraction data and the differences in refinement protocols, since in some cases the side-chain restraints can dominate the powder diffraction positional refinement.

3.1. Monomer and dimer conformations

A superposition of dimer 1 on dimer 2 by a least-squares procedure, minimizing the displacement of backbone atoms of all residues in common, resulted in a mean displacement of 0.528 Å and an r.m.s. displacement of 0.791 Å. Examination of Figs. 2(*a*) and 2(*b*) shows that with the exception of the last four residues of the C-terminus of the T-state B chain, few significant differences in conformation exist in the T-state monomers; excluding these four residues resulted in mean C^{α} displacements of 0.304 and 0.339 Å for the T-state A and B chains, respectively. Larger differences are observed for the

R^f-state monomers, as mean C^α displacements of 0.710 and 0.495 Å were calculated for the A and B chains, respectively. As can be seen in Fig. 2, displacements larger than 1.0 Å occur at the R^f-state residues GlyA1, GluA4, LeuA13, AsnA18 and ValB2. The mean B_{iso} for each R^f-state residue is found to be larger than its T-state counterpart; in dimer 2, the isotropic temperature factors of the first ten residues of the A chain and the first six residues of the B chain are larger than those of dimer 1. Also noted were numerous regions of 3σ $(F_o - F_c)$ density in the vicinity of the A6–A11 and A7–B7 disulfide bonds in dimer 2. These observations suggest that this region may possess multiple conformations which do not differ enough to allow them to be modeled separately.

A comparison of the two independent dimers to the dimer in 1trz as described above results in mean displacements of 0.596 and 0.671 Å for dimer 1 and dimer 2, respectively. Illustrated in Figs. 3(*a*) and 3(*b*) are the displacements at C^α for dimers 1 and 2 compared with 1trz. As noted above, the only displacements which exceed 1.0 Å for a T-state monomer are found at the C-terminus of the B chains. However, there are numerous large displacements for the R^f-state monomers, particularly in the first ten residues of the A chains and the first six residues of the B chains. These results show that not only are the R^f-state monomers different from each other, but they are also different from the R^f monomer in the room-temperature structure.

3.2. Hexamer stabilization and packing

Each of the two independent dimers generates an independent hexamer by virtue of the crystallographic threefold axis. A comparison of the C^α positions in the two dimers shows that the peptide backbones differ by a rotation of 9 (2)° about the *c* axis. A comparison of the two independent dimers to the

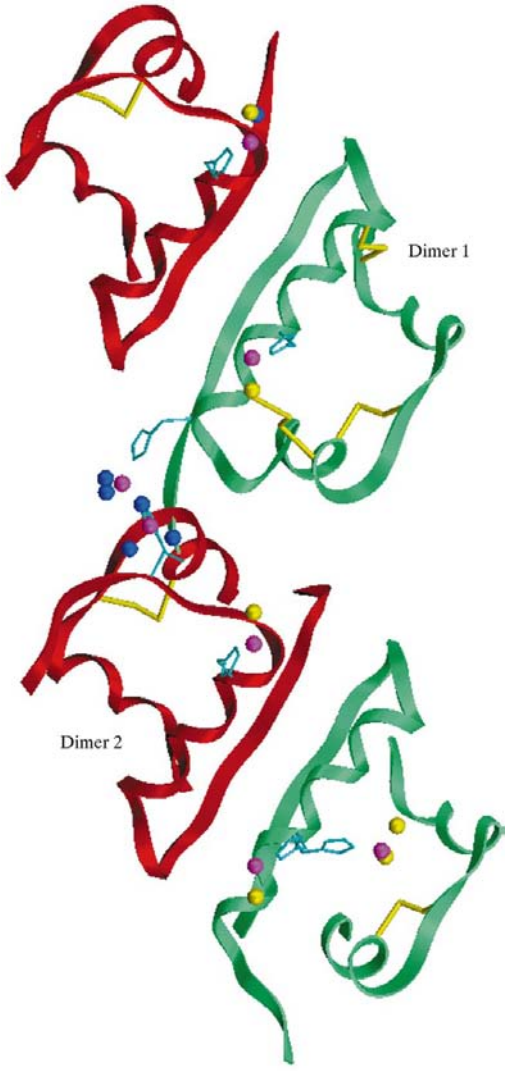

Figure 1
SETOR drawing (Evans, 1993) of the two independent $T_3R_3^f$ insulin dimers viewed perpendicular to the crystallographic threefold axis. T-state monomers are colored red, R^f-state monomers green, histidine side chains cyan, zinc ions magenta, chloride ions yellow and water molecules coordinated to zinc blue.

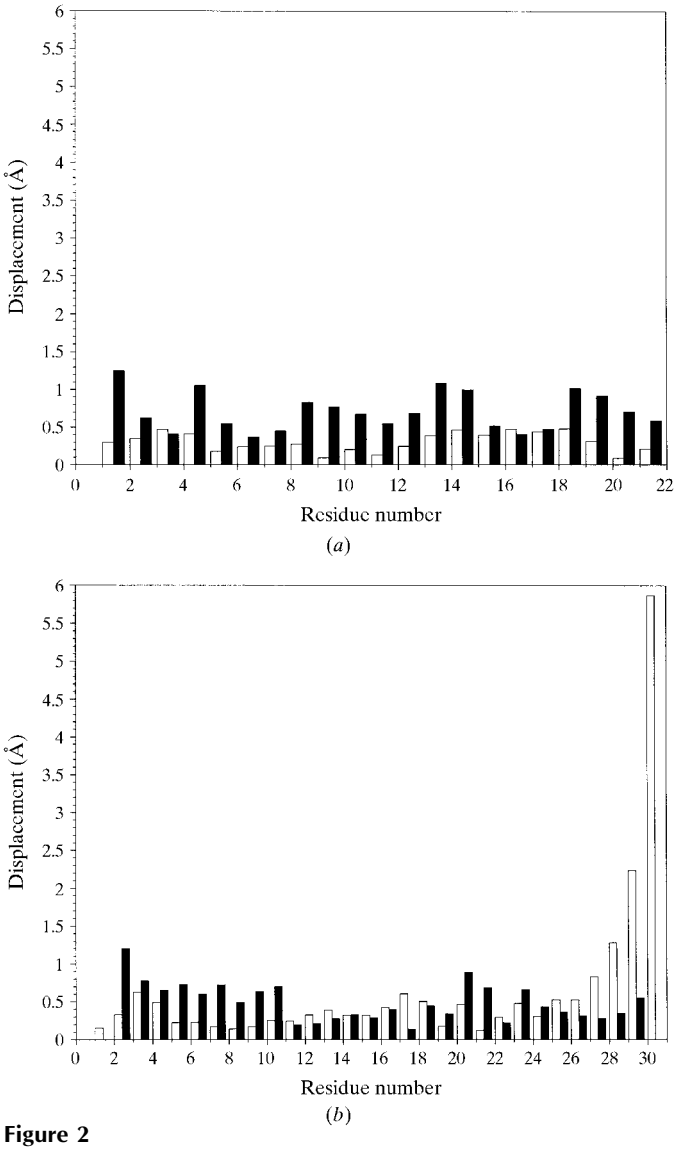

Figure 2
Histogram illustrating C^α displacements of (*a*) A chains and (*b*) B chains following a superposition of dimer 1 onto dimer 2. White bars are T-state monomers and black bars are R^f-state monomers.

room-temperature $T_3R_3^f$ dimer, PDB entry 1trz (Ciszak & Smith, 1994), shows that dimer 1 and dimer 2 are rotated 65 (5)° and 56 (4)°, in agreement with the difference in orientation of the two independent dimers. However, the ∼60° rotations result from the doubling of the *c* dimension of the unit cell and do not imply 60° molecular rotations. This is shown in Fig. 4, which is a schematic diagram of the packing of the hexamers in two unit cells of the room-temperature structure projected onto the *yz* plane. The hexamers labeled '*A*' and '*B*' in the lower unit cell occupy the obverse rhombohedral centering positions (2/3, 1/3, 1/3; 1/3, 2/3, 2/3). Doubling of the *c* axis transforms the structure from obverse to reverse, since hexamers '*B*' and '*C*' are now related to the hexamer at the origin by the reverse rhombohedral centering conditions (1/3, 2/3, 1/3; 2/3, 1/3, 2/3). Because the structures in the current study were refined in the obverse centering condition, the two dimers are related to the 1trz dimer by a rotation about the *c* axis of approximately 60°. Thus, the phase change and *c*-axis doubling result from rotations of dimers 1 and 2 by −5° and +4°, respectively, about the *c* axis relative to the room-temperature dimer.

Two sets of interactions between monomers stabilize the formation of the hexamer and are known as the dimer-forming and hexamer-forming residues (Baker *et al.*, 1988; Smith *et al.*, 1984). In the T_6 hexamer, dimer-forming hydrogen bonds exist in an antiparallel β-pleated sheet region consisting of residues B24–B26 in each monomer. These interactions are also present in the $T_3R_3^f$ hexamer. However, as a consequence of the movement of the B chain owing to the T→R transition, two additional intermonomer hydrogen bonds are produced between GluB13 and SerB9 and between TyrB16 and HisB5. The above hydrogen bonds exist in both the room-temperature and cryocooled crystals. Dimer-stabilizing hydrogen bonds involving GluB13 also exist and are discussed below.

Two hexamer-forming hydrogen bonds exist in the room-temperature structure of $T_3R_3^f$ insulin and both of these contacts are observed in the cryocooled crystals (Table 3). Owing to a small displacement of PheB1.3 relative to that of the room-temperature structure, an additional hydrogen bond is formed to ValB18.4. The GluB13 residues also contribute to hexamer-stabilizing interactions and are described below.

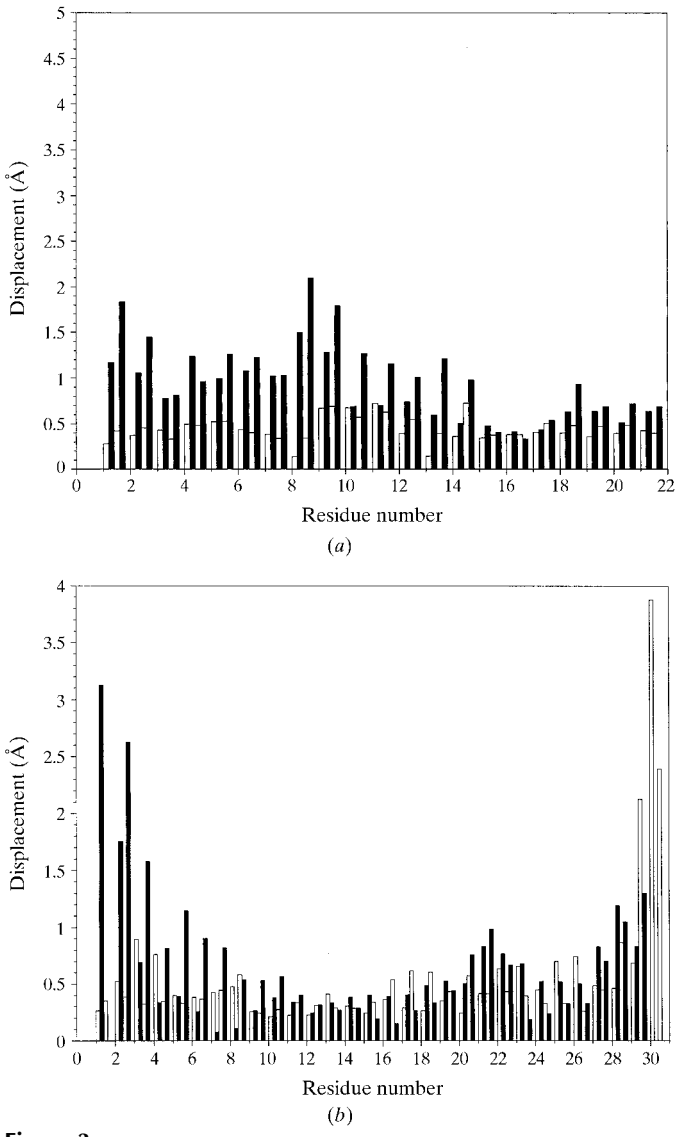

Figure 3
Histogram illustrating C^{α} displacements of (*a*) A chains and (*b*) B chains following a superposition of dimers 1 and 2 onto PDB entry 1trz. White bars are T-state monomers and black bars are R^f-state monomers; the first and second bars for each residue are dimer 1 while the third and fourth bars correspond to dimer 2.

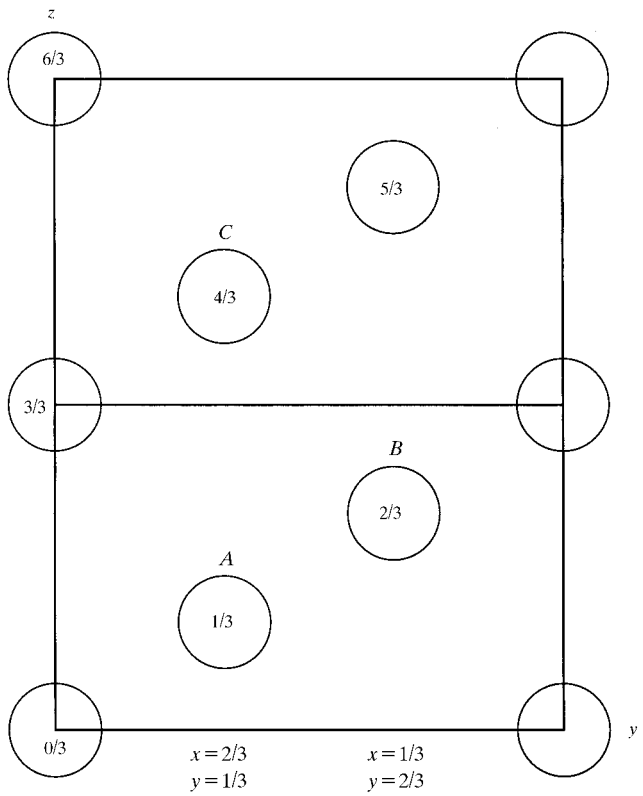

Figure 4
A schematic of hexamer packing in the room-temperature and doubled unit cell viewed perpendicular to the *bc* plane.

While numerous water-mediated hydrogen bonds exist between hexamers, only four interhexamer hydrogen bonds exist in the room-temperature structure. All four of these hydrogen bonds also exist in the cryocooled structure, but owing to the 9° rotation of one independent hexamer relative to the second an additional eight hydrogen bonds are produced (Table 3).

3.3. Zinc ion coordination

Three of the four axial zinc ions are tetrahedrally coordinated, while the fourth is statistically disordered with both tetrahedral and octahedral coordination. In all four cases, three of the ligands are the $N^{\varepsilon 2}$ atoms of three symmetry-related HisB10 side chains with Zn—N distances ranging from 1.97 to 2.03 Å. The fourth ligand in the tetrahedral case is a chloride ion, with Zn—Cl distances ranging from 2.12 to 2.25 Å. In the octahedral case, three symmetry-related water molecules complete the coordination sphere, with Zn—O distances of 2.42 Å.

In the room-temperature structures of $T_3R_3^f$ crystals grown in the presence of either chloride (Ciszak & Smith, 1994) or thiocyanate ion (Whittingham *et al.*, 1995), the off-axial zinc ion site or phenolic binding site is occupied by only water molecules. In the present study, a zinc ion with tetrahedral coordination is observed in the phenolic binding site in dimer 1 and is coordinated by $N^{\varepsilon 2}$ from a second orientation of HisB10.2, $N^{\varepsilon 2}$ of a symmetry-related HisB5.2 and two chloride ions at distances of 2.00, 2.02, 2.22 and 2.25 Å, respectively, as illustrated in Fig. 5. No zinc was found in the phenolic binding site in dimer 2, but rather a glycerol molecule and several water molecules, all with partial occupancies.

In the cryofrozen crystals, two partially occupied zinc ion sites were located between the two independent hexamers and each of the two zincs are tetrahedrally coordinated. The first zinc ion is coordinated by $N^{\varepsilon 2}$ (1.94 Å) of the first orientation of a disordered HisB5.1, HisB5.4 $N^{\varepsilon 2}$ (1.90 Å) and two chloride ions (2.24 and 2.40 Å). The second zinc is coordinated by $N^{\delta 1}$ (1.80 Å) of the second orientation of HisB5.1 and three water molecules (1.74, 2.17 and 2.19 Å). The coordination of these two zinc ions is illustrated in Fig. 6. While the electron density for the two zinc ions and histidine side chains was unambiguous [15 and 21σ ($F_o - F_c$) electron density for the zinc ions], adjacent regions of high electron density arising from disorder resulted in some difficulty in modeling and refining the other ligands, presumably owing to the presence of water molecules or other ions when the zinc ion is absent from its site.

3.4. GluB13 side-chain conformations

A comparison of the side-chain conformations and contacts involving the GluB13 side chains in T_6, $T_3R_3^f$ and R_6 hexamers suggests that these side chains play an important role in the T→R transition (Smith *et al.*, 2000). In the T_6 human insulin hexamer, the plane of each of the B13 carboxyl groups is nearly parallel to the crystallographic threefold axis and three symmetry-related short contacts of approximately 2.5 Å exist between the carboxyl O atoms (Baker *et al.*, 1988; Smith, Pangborn & Blessing, unpublished data), helping to stabilize the formation of the dimer. These short contacts have been interpreted as evidence for a protonated carboxyl group and a subsequent hydrogen bond or for the existence of a centered carboxylate–carboxylic acid hydrogen bond, both of which are in agreement with the observation that the pK_a of GluB13 is increased in hexameric insulin (Kaarsholm *et al.*, 1990).

In the room-temperature $T_3R_3^f$ hexamer (Ciszak & Smith, 1994; Whittingham *et al.*, 1995) (Fig. 7*a*), the planes of the T- or R-state GluB13 carboxyl groups are nearly parallel or perpendicular to the crystallographic threefold axis, respectively, and the closest contact between the carboxyl groups is 3.07 Å, which does not conclusively suggest the presence of a hydrogen bond. At the same time, the T-state GluB13 carboxyl group accepts a proton from SerB9 O^{γ}, a dimer-stabilizing interaction. The conformations of the T-state GluB13 side chains are very similar in both the room-temperature and low-temperature $T_3R_3^f$ hexamers. In the cryocooled crystals, the GluB13 side chains of both R-state monomers are disordered and exist in two discrete conformations (Figs. 7*b* and 7*c*) with the planes of the carboxyl groups nearly perpendicular to the threefold axis, as observed in the room-temperature structure.

In dimer 1, a dimer-stabilizing hydrogen bond exists between SerB9.2 O^{γ} and GluB13.1 $O^{\varepsilon 1}$, while the closest contact between B13 carboxyl groups is 3.17 Å (Fig. 7*b*). A similar dimer-stabilizing interaction exists in dimer 2, where GluB13.3 $O^{\varepsilon 1}$ accepts a hydrogen bond from SerB9.4 O^{γ}. The two alternate conformations of GluB13.4 are dissimilar to that observed in dimer 1 as well as that of the room-temperature structure. As a result of this difference in conformation, a short contact of 2.54 Å, a hexamer-stabilizing interaction, exists between $O^{\varepsilon 1}$ of one alternate orientation of GluB13.4 and GluB13.3 $O^{\varepsilon 2}$ (Fig. 7*c*), for which both side chains have very well defined electron densities at 2.5σ in the ($2F_o - F_c$) electron-density maps. In the second glutamate side-chain conformation of GluB13.4, $O^{\varepsilon 2}$ makes a 2.73 Å contact to the carbonyl O atom of SerB9.3, contributing to the stability of the dimer. Thus, the carboxyl group of GluB13.4 appears to be protonated in both of its alternate conformations.

4. Conclusions

The results from this structural study show that when cryocooled, hexameric $T_3R_3^f$ insulin undergoes a phase transition. As a result of rotations of −5° and +4° of two translationally related hexamers, the *c* axis of the unit cell is doubled. This phase transition was also observed in powder diffraction experiments performed at room temperature (Von Dreele *et al.*, 2000), which eliminates temperature as the cause of the phase change. In the case of the powder diffraction experiments, the pressure resulting from the mechanical grinding of the sample induced the same *c*-doubling phase transition, but the sample reverts back to the original single *c*-axis form after several days. Diffraction data measured from single crystals at room temperature did not exhibit a change in phase, but data

from cryofrozen crystals surrounded by a cryoprotectant drop or a thin layer of paraffin oil did show *c* doubling at 100 K. Based on these results and the powder diffraction results, we suggest that the observed phase transition is not directly a consequence of reduced temperature, but rather a result of pressure from the contraction of the cryoprotectant drop, the contraction of the thin layer of paraffin oil or the contraction of the crystal itself.

Associated with the doubling of the *c* axis, two additional zinc ions appear to be trapped and bind between the two independent dimers through coordination to HisB5 residues and chloride or water molecules. In one of the independent dimers, a zinc ion is found in the 'phenolic binding' site where it is coordinated to HisB5, HisB10 and two chloride ions. This same site in the second dimer was found to contain a glycerol molecule and several water molecules.

In contrast to other published $T_3R_3^f$ insulin hexamers (Ciszak & Smith, 1994; Whittingham *et al.*, 1995), one of the GluB13 residues, located in the central portion of the hexamer, appears to be protonated. Unlike the protonated GluB13 in T_6 insulin, where the hydrogen bond between carboxyl groups helps to stabilize the formation of the dimer, the hydrogen bond between carboxyl groups in the current study stabilizes the formation of the hexamer.

One frequently hears informal reports regarding doubling of cell axes following freezing, but many crystallographers discard such samples and continue searching for crystals which when frozen closely mimic the room-temperature unit cells (P. L. Howell, private communication; S. A. Ealick, private communication). T_6 human insulin also undergoes a change in conformation of one of the N-termini of the B chains when frozen, which amounts to a shift of nearly 8 Å of the C^{α} of PheB1. Since there are few examples of structures that have been determined at both room temperature and cryotemperature, one must keep in mind that the structure and conformation at cryotemperature are not necessarily those that would be observed at room temperature.

The authors wish to thank Dr Marianna Long and Ms Vickie King of the PCF at the University of Alabama, Birmingham for setting up the microgravity crystal-growth experiments and Lilly Research Laboratories for a generous gift of recombinant human insulin. The authors also wish to thank Drs P. Lynne Howell and Yuri Lobsanov of the Hospital for Sick Children, Toronto, Ontario for the use of their R-AXIS IV^{++} and their assistance in performing the diffraction experiments on crystals coated with paraffin oil. The microgravity crystallization experiments were supported by NASA grant NCC8-126 to Larry DeLucas, while the data measurement, processing and refinement were supported by NIH Grant GM56829.

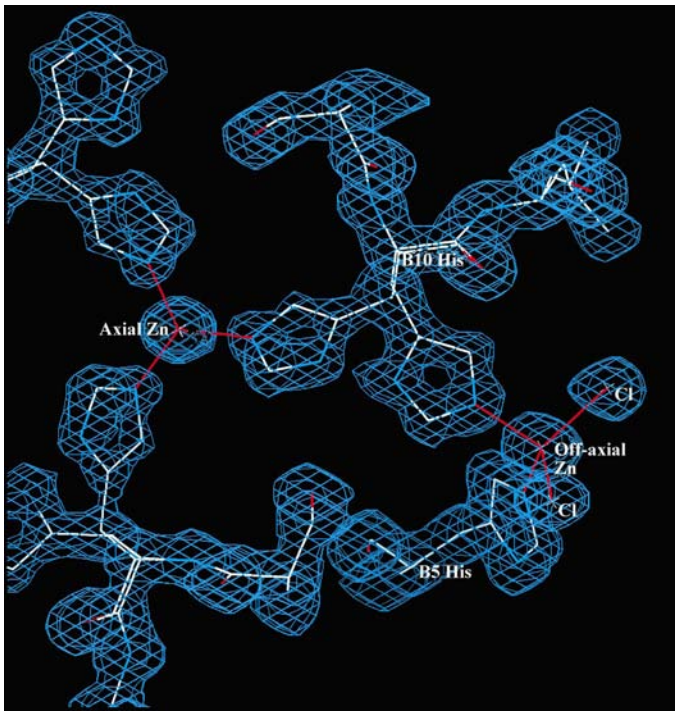

Figure 5
The coordination and σ_A-weighted ($2F_o - F_c$) electron densities for the R^f-state zinc ions in dimer 1 as viewed parallel to the crystallographic threefold axis. Since the chloride ion, which completes the tetrahedral coordination to the axial zinc ion, lies directly under the zinc, only three bonds (red lines) to HisB10.2 are illustrated. A second orientation of HisB10.2, a symmetry-related HisB5.2 and two chloride ions form bonds (red lines) to the off-axial zinc ion.

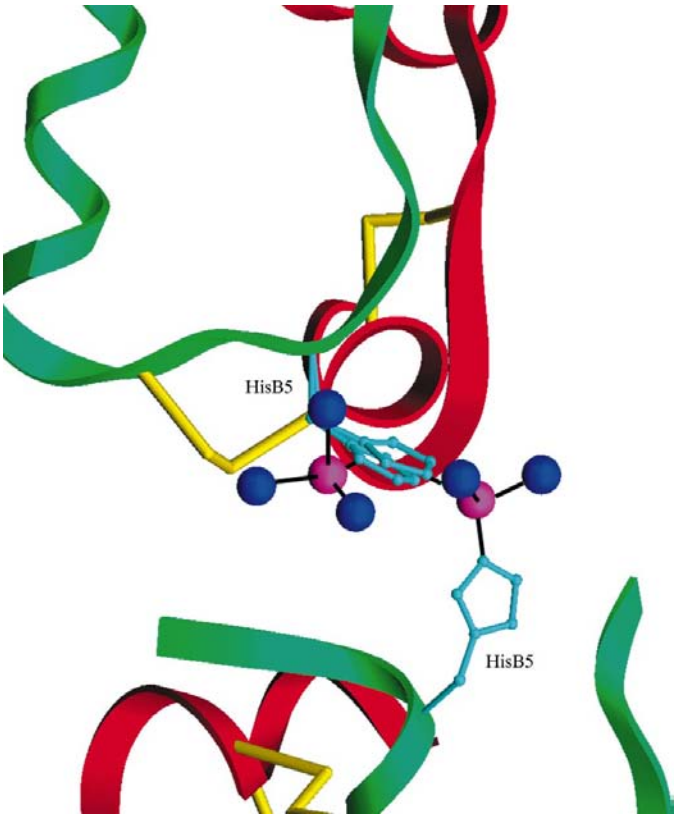

Figure 6
SETOR drawing (Evans, 1993) of the interface between the two independent dimers, illustrating the coordination to the two zinc ions. A chains are colored red, B chains green, water molecules dark blue, zinc ions magenta, histidine side chains cyan and disulfide bridges yellow.

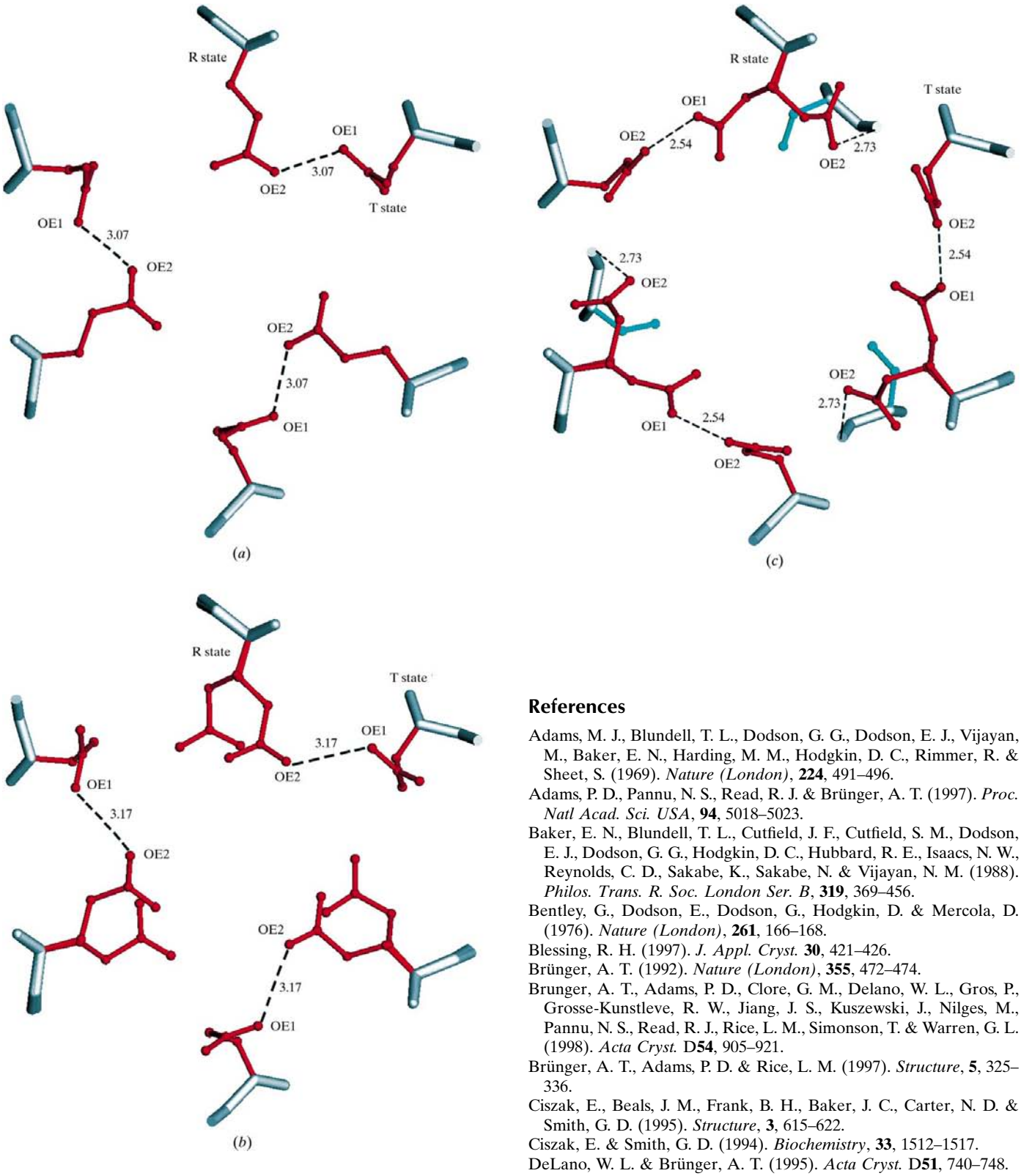

Figure 7
Interactions between the GluB13 side chains in (*a*) 1trz; (*b*) hexamer 1 of the present study and (*c*) hexamer 2 of the present study. In (*c*), the side chains of SerB9.3 are colored cyan; the black dashed lines illustrate the 2.54 Å contact between GluB13.4 $O^{\varepsilon 1}$ and GluB13.3 $O^{\varepsilon 2}$ and the 2.73 Å contact between the carbonyl O of SerB9.3 and $O^{\varepsilon 2}$ of the second alternate orientation of GluB13.4.

References

Adams, M. J., Blundell, T. L., Dodson, G. G., Dodson, E. J., Vijayan, M., Baker, E. N., Harding, M. M., Hodgkin, D. C., Rimmer, R. & Sheet, S. (1969). *Nature (London)*, **224**, 491–496.

Adams, P. D., Pannu, N. S., Read, R. J. & Brünger, A. T. (1997). *Proc. Natl Acad. Sci. USA*, **94**, 5018–5023.

Baker, E. N., Blundell, T. L., Cutfield, J. F., Cutfield, S. M., Dodson, E. J., Dodson, G. G., Hodgkin, D. C., Hubbard, R. E., Isaacs, N. W., Reynolds, C. D., Sakabe, K., Sakabe, N. & Vijayan, N. M. (1988). *Philos. Trans. R. Soc. London Ser. B*, **319**, 369–456.

Bentley, G., Dodson, E., Dodson, G., Hodgkin, D. & Mercola, D. (1976). *Nature (London)*, **261**, 166–168.

Blessing, R. H. (1997). *J. Appl. Cryst.* **30**, 421–426.

Brünger, A. T. (1992). *Nature (London)*, **355**, 472–474.

Brunger, A. T., Adams, P. D., Clore, G. M., Delano, W. L., Gros, P., Grosse-Kunstleve, R. W., Jiang, J. S., Kuszewski, J., Nilges, M., Pannu, N. S., Read, R. J., Rice, L. M., Simonson, T. & Warren, G. L. (1998). *Acta Cryst.* D**54**, 905–921.

Brünger, A. T., Adams, P. D. & Rice, L. M. (1997). *Structure*, **5**, 325–336.

Ciszak, E., Beals, J. M., Frank, B. H., Baker, J. C., Carter, N. D. & Smith, G. D. (1995). *Structure*, **3**, 615–622.

Ciszak, E. & Smith, G. D. (1994). *Biochemistry*, **33**, 1512–1517.

DeLano, W. L. & Brünger, A. T. (1995). *Acta Cryst.* D**51**, 740–748.

Derewenda, U., Derewenda, Z., Dodson, E. J., Dodson, G. G., Reynolds, C., Sparks, K., Smith, G. D. & Swenson, D. C. (1989). *Nature (London)*, **338**, 594–596.

Evans, S. V. (1993). *J. Mol. Graph.* **6**, 244–245.

Kaarsholm, N. C., Havelund, S. & Hougaard, P. (1990). *Arch. Biochem. Biophys.* **283**, 496–502.

Kaarsholm, N. C., Ko, H. & Dunn, M. F. (1989). *Biochemistry*, **28**, 4427–4435.

Laskowski, R. A., MacArthur, M. W., Moss, D. S. & Thornton, J. M. (1993). *J. Appl. Cryst.* **26**, 283–291.
Otwinowski, Z. & Minor, W. (1997). *Methods Enzymol.* **276**, 307–326.
Pannu, N. S. & Read, R. J. (1996). *Acta Cryst.* A**52**, 659–668.
Read, R. J. (1986). *Acta Cryst.* A**42**, 140–149.
Rice, L. M. & Brünger, A. T. (1994). *Proteins Struct. Funct. Genet.* **19**, 277–290.
Sack, J. S. (1988). *J. Mol. Graph.* **6**, 244–245.
Schlichtkrull, J. (1958). *Insulin Crystals.* Copenhagen: Munksgaard.
Smith, G. D. (1993). *PROFIT. A Locally Written Program for Orienting one Protein Molecule onto Another by a Least-Squares Procedure*. Hauptman–Woodward Medical Institute, Buffalo, USA.
Smith, G. D. (1998). *J. Mol. Struct.* **469**, 71–80.
Smith, G. D. & Ciszak, E. (1994). *Proc. Natl Acad. Sci. USA*, **91**, 8851–8855.
Smith, G. D., Ciszak, E., Magrum, L. A., Pangborn, W. A. & Blessing, R. H. (2000). *Acta Cryst.* D**56**, 1541–1548.
Smith, G. D., Ciszak, E. & Pangborn, W. A. (1996). *Protein Sci.* **5**, 1502–1511.
Smith, G. D. & Dodson, G. G. (1992). *Proteins Struct. Funct. Genet.* **14**, 401–408.
Smith, G. D., Swenson, D. C., Dodson, E. J., Dodson, G. G. & Reynolds, C. D. (1984). *Proc. Natl Acad. Sci. USA*, **81**, 7093–7097.
Von Dreele, R. B., Stephens, P. W., Smith, G. D. & Blessing, R. H. (2000). *Acta Cryst.* D**56**, 1549–1553.
Whittingham, J. L., Chaudhurri, S., Dodson, E. J., Moody, P. C. E. & Dodson, G. G. (1995). *Biochemistry*, **34**, 15553–15563.